Emergence of d_{xy}-wave superconductivity in a doped two-leg diagonal ladder

Jie Hou,[1] Ting-Kuo Lee,[2] Jie Lou,[1,3] and Yan Chen[1,3]
[1]*Department of Physics and State Key Laboratory of Surface Physics, Fudan University, Shanghai 200433, China*
[2]*Institute of Physics, Academia Sinica, Nankang, Taipei 11529, Taiwan*
[3]*Collaborative Innovation Center of Advanced Microstructures, Nanjing 210093, China*

(Received 19 November 2018; revised manuscript received 5 February 2019; published 12 March 2019)

We propose a doped two-leg spin-1/2 diagonal ladder model (or a composite spin model) to simulate a doped spin-1 chain. By using the density matrix renormalization group method for an open chain, we find that the ground state hosts a dominant singlet d_{xy}-wave superconducting correlation with features similar to those of the spin-1 Haldane phase. Meanwhile, we apply the renormalized mean-field theory to the model and obtain a d_{xy}-wave superconducting state. The superconducting order exhibits a domelike shape as a function of hole concentration δ. Our work provides a physical understanding of the origin of d_{xy} pairing symmetry, which originates from antiferromagnetic Heisenberg interaction in the diagonal direction, and the intrachain hopping term makes it stable.

DOI: 10.1103/PhysRevB.99.094510

I. INTRODUCTION

It is well known that the ground state of the antiferromagnetic spin-1 Heisenberg chain is the Haldane phase with symmetry-protected gapless edge states [1–3]. If a finite hole density is introduced, the resulting model with kinetic energy and antiferromagnetic interaction exhibits similar topological properties [4]. The spin sector is gapped, and the charge sector is gapless in the large-(t/J) regime. The gapless Haldane phase was also found in a topological superconducting chain recently [5]. To further explore the doped spin-1 chain, it is instructive to study an equivalent two-leg spin-1/2 ladder model. Quasi-one-dimensional (quasi-1D) systems such as a two-leg ladder have been of great interest because they serve as a good platform to further study two-dimensional models [6,7]. Although they are essentially 1D systems, two-dimensional (2D) characteristics can emerge because the interchain degrees of freedom appear. In addition, these systems are much easier to solve than 2D models, especially using the density matrix renormalization group (DMRG) method [8,9]. For example, the t-J model on a two-leg square ladder has been attracting continuous attention for both theoretical and experimental reasons [6,10–13].

A typical example to simulate a spin-1 chain is a spin-1/2 ladder model with a strong interchain ferromagnetic Heisenberg interaction in addition to an intrachain antiferromagnetic interaction [14]. When doped with holes, this model will exhibit an exotic ground state, which is a symmetry-protected topological Luttinger liquid with a power-law decaying superconducting (SC) pair correlation [15,16]. The superconductivity exhibits d_{xy} orbital symmetry in this model, and the spin sector of the Cooper pair is a singlet. This pairing symmetry was found in some ladder models previously [17–19], but its physical origin remains unclear.

To further investigate the properties of the doped Haldane phase and d_{xy} superconductivity, in this paper we study a doped two-leg spin-1/2 diagonal ladder model, as depicted in Fig. 1. The undoped spin system is called a diagonal ladder model or a composite spin model [20,21]. The low-lying states are identical to those of a spin-1 chain. When the doped holes are allowed to move along the chain, we find that the ground state hosts features similar to those of the Haldane phase, including the spin gap, edge states, and twofold degeneracy in the entanglement spectrum. In addition, it belongs to the Luther-Emery phase [22] and the Luttinger parameter $K_\rho > 1$ at low doping levels. This diagonal ladder model has negative binding energy and a power-law decaying d_{xy}-wave-dominant superconducting correlation, which is the same as that obtained in the previous studies [15,16] with ferromagnetic vertical interchain interaction but in the absence of antiferromagnetic diagonal interchain interaction. This pairing symmetry seems to be more natural in our model because the paired electrons have direct Heisenberg interaction.

To understand the above DMRG results with more insight, we use the renormalized mean-field theory (RMFT) [23] to solve this problem. RMFT method is based on the Gutzwiller approximation of the projected BCS wave function (Anderson's resonating valence bond (RVB) variational wave function [24]), which has been widely employed to study 2D and quasi-1D t-J models [11,23,25–28]. By using this method, we find that the pairing symmetry is also a singlet d_{xy} wave. The superconducting order parameter exhibits a domelike shape as a function of hole doping level. By analyzing the bond and pair mean fields, our work provides a physical understanding of the origin of d_{xy}-wave pairing symmetry. The d_{xy}-wave pairing directly comes from the Heisenberg interaction J in the diagonal direction. Meanwhile, it is the hopping term that stabilizes such pairing symmetry.

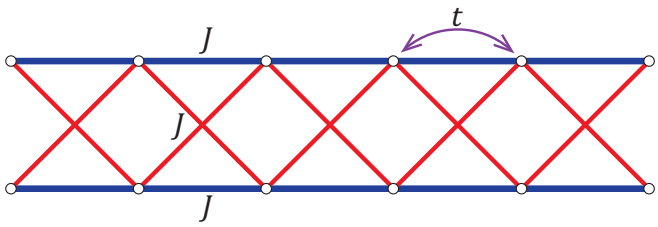

FIG. 1. The structure of the two-leg diagonal ladder model. We have both t and J terms on the intrachain bonds (blue lines), with only the J term on the interchain bonds (red lines).

The Hamiltonian of the doped two-leg diagonal ladder model is

$$H = -t \sum_{i,\alpha,\sigma} (c^{\dagger}_{\alpha,i,\sigma} c_{\alpha,i+1,\sigma} + \text{H.c.}) + J \sum_{i,\alpha,\alpha'} \boldsymbol{S}_{\alpha,i} \cdot \boldsymbol{S}_{\alpha',i+1}. \quad (1)$$

Here the operator $c^{\dagger}_{\alpha,i,\sigma}$ creates a fermion with spin σ at site i on chain α ($\alpha = 1, 2$). $\boldsymbol{S}_{\alpha,i}$ denotes the spin-1/2 operators. The Hamiltonian contains the intrachain hopping term as well as the horizontal and diagonal antiferromagnetic Heisenberg interaction terms. In the Hilbert space, one site occupied with two electrons is prohibited by imposing $\sum_{\sigma} c^{\dagger}_{\alpha,i,\sigma} c_{\alpha,i,\sigma} \leqslant 1$. In this paper we set $t = 1$ and $J = 0.3$ unless noted otherwise. The doping level is defined as $\delta = N_h/N$, N_h is the number of holes, and N is the number of lattice sites. In our ladder system $N = L \times 2$, and L is the length of the system.

This paper is organized as follows. In Sec. II we show the ground-state properties found in DMRG, including the spin gap, edge state, binding energy, charge density oscillations, and pair-pair correlations. After that, in Sec. III the superconductivity is calculated and analyzed in detail using RMFT. Section IV includes some discussion of our results. Finally, our conclusions are presented in Sec. V.

II. DMRG RESULTS

The DMRG calculation is performed with ITENSOR library [29] based on matrix product state formalism. The system size is up to $L = 240$, and the hole density is up to $\delta = 0.40$. Open boundary conditions (OBCs) are always used. We keep up to $m = 3000$ states with a truncation error less than 10^{-7} in most calculations. During the sweeping process, the total S_z is fixed at zero except for the calculation of the spin gap. In some quantitative analysis, we extrapolate the result to the $m = \infty$ limit, which corresponds to an exact wave function.

A. Spin and charge properties

Figure 2 illustrates the spin-1 and spin-2 excitation gaps ($\Delta_{S=1}, \Delta_{S=2}$) for several L at $\delta = 0.05$ hole doping. Here $\Delta_S = E_0(S_z = S) - E_0(S_z = 0)$, and $E_0(S_z)$ is the ground-state energy of the system with total S_z. We can see that $\Delta_{S=1} = 0$ and $\Delta_{S=2}$ has a finite value when $1/L \to \infty$. The inset displays the expectation value of $S^z_i = S^z_{1,i} + S^z_{2,i}$ and hole density $n^h_i = 1 - n_{1,i}$ ($n_{1,i} = n_{2,i}$) in a 200×2 lattice with two holes ($\delta = 0.005$) in the ground state of the sector $S^z_{tot} = 1$. It is easy to see the existence of edge spin $S = 1/2$ at two ends of the system. When the doping level is higher (up to 0.40), we find that the edge states still exist (Fig. 14 below shows the $\delta = 0.15$ result). Therefore, in Fig. 2 $\Delta_{S=1} = 0$ is the result of two gapless edge states, and $\Delta_{S=2}$ represents the bulk spin gap. These results confirm that the spin sector of our two-leg model is very similar to the doped Haldane phase in previous work [15,16]. In Fig. 3 we show the values of the spin gap as a function of doping in the left axis. The system size is $L = 80$, and the state kept is $m = 1000$. $\Delta_{S=1} = 0$ always holds, and the bulk spin gap $\Delta_{S=2}$ exists in this wide doping range. It gradually decreases with δ, probably because more charge fluctuations are introduced with the increasing of holes.

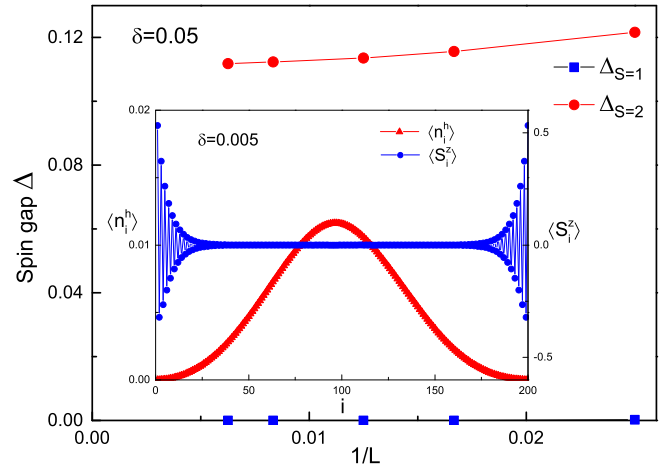

FIG. 2. The spin gap Δ_S with $\delta = 0.05$ hole doping for different ladder lengths L. The blue (red) symbols mark the spin-1 (spin-2) excitation gap. $\Delta_{S=1} = 0$, and $\Delta_{S=2}$ has a finite value. Inset: The distribution of n^h_i (red symbols) and S^z_i(blue symbols) in a 200×2 system with two holes (doping level $\delta = 0.005$) in the sector $S^z_{tot} = 1$. Gapless edge states appear at both ends.

As for the charge sector, it is known that the doped Haldane phase is a Luttinger liquid [15]. Here we use several ways to support this picture and extract the Luttinger parameter K_ρ

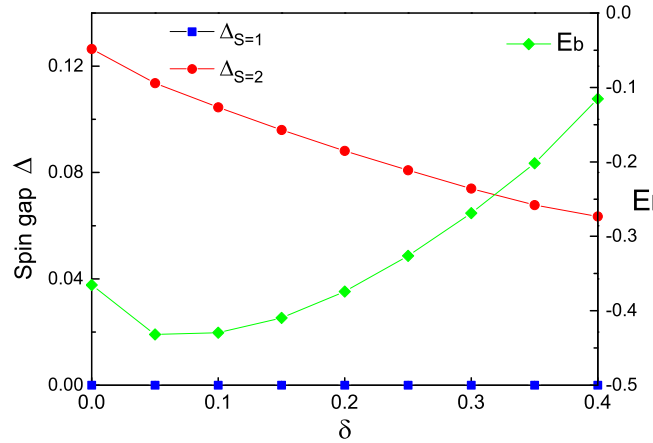

FIG. 3. Spin gap $\Delta_{S=1}$, $\Delta_{S=2}$ (left axis) and binding energy E_b (right axis) as a function of doping in an 80×2 system. $\Delta_{S=1} = 0$ and $\Delta_{S=2} > 0$ in this doping range. The binding energy $E_b < 0$ shows the existence of pairing tendency.

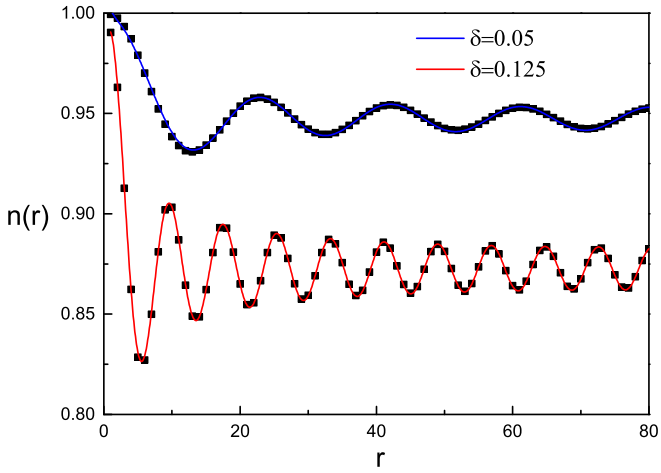

FIG. 4. Local electron density of sites 1–80 on one chain in a 160×2 system at doping levels $\delta = 0.05$ and 0.125. The scatter points are from DMRG results. The blue and red lines are the fit curves using Eq. (2). The wavelength λ is around $1/\delta$.

[30,31]. The OBC in DMRG naturally leads to charge density oscillations in the ground state, namely, Friedel oscillations. We find that the charge density wave (CDW) on either chain behaves as $A(r)\cos(Q \cdot r + \theta)$, with the wave vector $Q = 2\pi\delta$ and the wavelength $\lambda = 1/\delta$. For example, the distribution of the charge density in the inset of Fig. 2 shows a $\lambda = 200$ wavelength because the doping level $\delta = 0.005$. The reason is that the hole density δ determines k_F for a Luttinger liquid. The amplitude of CDW decays away from the boundaries with a power law. Considering the finite-size effect, the electron density in the left or right half of the system can be described by [30,32]

$$n(r) = n_0 + A\cos(Q \cdot r + \theta)\left(\frac{2L}{\pi}\sin\frac{\pi r}{L}\right)^{-K_\rho/2}. \quad (2)$$

In Fig. 4 we show the local electron density of the sites 1–80 on one chain in a 160×2 system at doping levels $\delta = 0.05$ and 0.125 by keeping $m = 2000$ state. The scatter points represent the calculated charge density, and the blue and red lines are the fitting curves. The wavelength of the CDW is about 20 for $\delta = 1/20$ and 8 for $\delta = 1/8$, as expected. We obtain the Luttinger parameter K_ρ from these fittings and then extrapolate to the limit of truncation error $\epsilon = 0 (m \to \infty)$. K_ρ at different doping levels is shown in Table I (CDW row). It is larger than 1 and decreases with doping.

TABLE I. K_ρ at different dopings extracted from the CDW and SC pair correlations. $K_\rho > 1$ means that the SC correlation plays a dominant role.

	Doping			
	0.05	0.10	0.125	0.142
CDW	1.51	1.38	1.34	1.31
SC	1.47	1.34	1.23	1.16

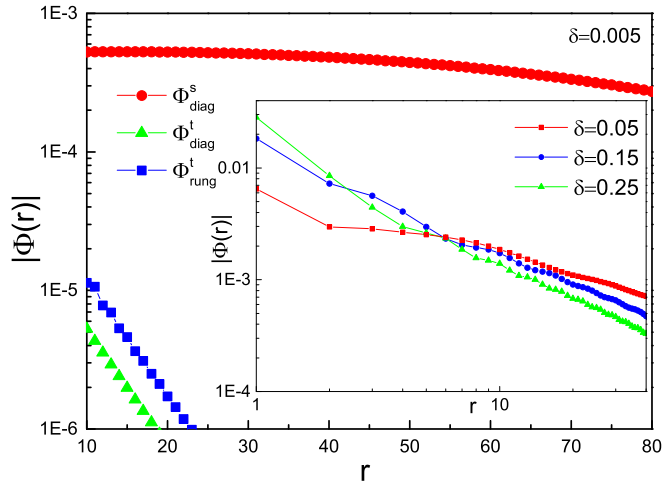

FIG. 5. The absolute value of pair-pair correlations along the rung and diagonal direction as a function of r in a 200×2 system with two holes. The diagonal singlet channel is the most prominent. Inset: The diagonal singlet pair correlations at different doping levels in a 100×2 system. The nearly straight line at a log-log scale exhibits the power-law decaying behavior.

B. Superconducting properties

To explore the pairing tendency, we first calculate the two-hole binding energy $E_b = E_G(N) + E_G(N-2) - 2E_G(N-1)$, where $E_G(M)$ denotes the ground-state energy of the system with M electrons. Figure 3 shows the binding energy in the right axis at several doping levels with $L = 80$. $E_b < 0$ represents the tendency of the fermion pair formation in this wide doping range. With the increase in δ, its magnitude first increases, then drops continuously, indicating that the pairing strength achieves a maximum at moderate doping.

To further investigate the superconducting properties, we calculate the singlet and triplet Cooper pair correlation functions. The correlation function is defined as

$$\Phi^{s,t}_{ab}(r) = \langle \hat{\Delta}^{s,t}_a(i)\hat{\Delta}^{s,t}_b(i+r)^\dagger \rangle, \quad (3)$$

where the pair operators in the singlet and triplet channels are defined as

$$\hat{\Delta}^s_a(i) = \frac{1}{\sqrt{2}}\sum_\sigma \sigma \hat{c}_{i,\sigma}\hat{c}_{i+a,-\sigma},$$
$$\hat{\Delta}^t_a(i) = \frac{1}{\sqrt{2}}\sum_\sigma \hat{c}_{i,\sigma}\hat{c}_{i+a,-\sigma}, \quad (4)$$

where $a = y, (x \pm y)$ denote the sites along the rung and diagonal directions, respectively. In Fig. 5 we show the local rung $(a = y, b = y)$ and the diagonal $(a = x \pm y, b = x \pm y)$ pairing correlations in a 200×2 system doped with two holes. It is found that the singlet diagonal pairing is decreasing slowly and the triplet rung or triplet diagonal channel is decaying exponentially. Furthermore, the correlations in the diagonal direction with $a = x + y, b = x + y$ and $a = x + y, b = x - y$ have opposite signs with the same absolute value, which corresponds to the feature of d_{xy}-wave pairing symmetry. This result is similar to the model [15,16] without diagonal antiferromagnetic interaction. In the inset of Fig. 5 we show

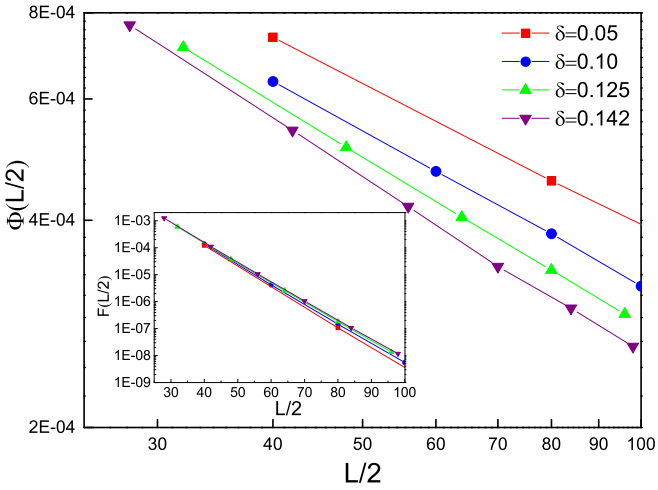

FIG. 6. Pair-pair correlation as a function of the system size on a log-log plot at several doping levels. The straight line shows the power-law decaying behavior. In the inset, we show the spin-spin correlation function on a log-linear plot. The straight line shows the exponential decaying behavior.

the singlet diagonal pair-pair correlations as a function of r in the log-log scale at several doping levels in a 100×2 system. The nearly straight lines further confirm the power-law decaying behavior of the correlations. To minimize the influence of the OBCs, we calculate the correlation functions in the middle range of the system ($L/4$ to $3L/4$) and show the average value for a fixed r [33].

The determination of K_ρ from the decay of the correlation functions is expected to be less reliable than from local densities [32]. To calculate the Luttinger parameter carefully, we extract the correlation function at given sites in systems with different sizes [31]. Note that the pair-pair correlation function should decay as

$$\Phi(r) \propto r^{-1/K_\rho}. \tag{5}$$

In practice we calculate $\Phi(\frac{L}{2}) = \langle \hat{\Delta}(\frac{L}{4})\hat{\Delta}(\frac{3L}{4})^\dagger \rangle$ and extrapolate to the $\epsilon = 0$ limit for a fixed system. Then we use different system sizes to obtain the corresponding correlation functions. Doping level and system size are carefully chosen to ensure that the charge density at the site $L/4$ and $3L/4$ is a local maximum. Therefore, the influence of the CDW on the decaying behavior of superconducting correlation is minimized. In Fig. 6 we show the d_{xy}-wave superconducting correlation as a function of L in a double-logarithmic plot at several doping levels. The straight lines confirm the power-law behavior. We extract K_ρ from the slope according to Eq. (5). The values are listed in Table I (SC row). In general, they are close to the values calculated from the charge density oscillations. Both methods show that $K_\rho > 1$, which means the system is dominated by the d-wave pair correlations rather than CDW correlations [32]. Combining spin, charge, and pairing properties, we confer that the ground state of the doped Haldane phase is a Luther-Emery liquid, which is similar to some weakly doped t-J or Hubbard square ladders [32,34]. In the inset of Fig. 6 we also show the spin-spin correlation function $F(L/2) = |\langle \vec{S}_{L/4} \cdot \vec{S}_{3L/4} \rangle|$ at different system sizes at several doping levels. The straight line represents the correlation is decaying exponentially, which is consistent with the feature of a bulk spin gap.

III. Renormalized Mean-Field Theory

A. Method

To obtain an intuitive and qualitative understanding of the superconducting properties, we use RMFT to handle this problem. The no-double-occupancy constraint is relaxed by adding renormalized Gutzwiller factors g_t before the intra-chain hopping t term and g_s before the superexchange J term. Therefore, the renormalized Hamiltonian defined in the Hilbert space without the constraint can be written as

$$\tilde{H} = -g_t t \sum_{\langle ij \rangle_\parallel, \sigma} (c^\dagger_{i,\sigma} c_{j,\sigma} + \text{H.c.}) + g_s J \sum_{\langle ij \rangle_{\parallel,\times}} \boldsymbol{S}_i \cdot \boldsymbol{S}_j. \tag{6}$$

Here $\langle ij \rangle_\parallel$ means that i and j are two nearest-neighbor sites in the horizontal direction (blue line in Fig. 1), and $\langle ij \rangle_\times$ means that i and j are two sites in the diagonal direction (red line in Fig. 1). For nonmagnetic states the Gutzwiller factors are given as

$$g_t = \frac{2\delta}{1+\delta}, \quad g_s = \frac{4}{(1+\delta)^2}, \tag{7}$$

where δ is the hole concentration. Then we define the pair field and bond field between two sites as

$$\begin{aligned} \Delta^v_{ij\sigma} &= \sigma \langle \Psi_0 | c_{i\sigma} c_{j-\sigma} | \Psi_0 \rangle, \\ \chi^v_{ij\sigma} &= \langle \Psi_0 | c^\dagger_{i\sigma} c_{j\sigma} | \Psi_0 \rangle. \end{aligned} \tag{8}$$

Here $|\Psi_0\rangle$ is the unprojected ground-state wave function of Hamiltonian (6); ij denotes two neighboring sites in horizontal ($\parallel$) or diagonal ($\times$) direction. Then the superconducting gap order parameter and the bond order parameter which correspond to the expectation values of the operators in the projected wave function $|\Psi\rangle$ [ground state of Hamiltonian (1)] are calculated by

$$\begin{aligned} \Delta^{SC}_{ij} &= \frac{1}{2} \sum_\sigma \sigma \langle \Psi | c_{i\sigma} c_{j-\sigma} | \Psi \rangle = \frac{1}{2} g_t \sum_\sigma \Delta^v_{ij\sigma}, \\ K_{ij} &= \frac{1}{2} \sum_\sigma \langle \Psi | c^\dagger_{i\sigma} c_{j\sigma} | \Psi \rangle = \frac{1}{2} g_t \sum_\sigma \chi^v_{ij\sigma}. \end{aligned} \tag{9}$$

The mean-field Hamiltonian can be written as

$$\begin{aligned} H_{MF} = &-g_t t \sum_{\langle ij \rangle_\parallel, \sigma} \left(c^\dagger_{i,\sigma} c_{j,\sigma} + \text{H.c.} \right) \\ &- \frac{3}{4} g_s J \sum_{\langle ij \rangle_{\parallel,\times}, \sigma} \left(\chi^v_{ij\sigma} c^\dagger_{i\sigma} c_{j\sigma} + \Delta^v_{ij\sigma} c^\dagger_{i\sigma} c^\dagger_{j-\sigma} + \text{H.c.} \right) \\ &- \mu \sum_{i\sigma} c^\dagger_{i\sigma} c_{i\sigma}. \end{aligned} \tag{10}$$

Here μ is the chemical potential for controlling the hole-doping concentration. Then we can solve the Bogoliubov–de Gennes (BdG) equations self-consistently. The system size is 100×2, and we confirm the convergence of the solution if the

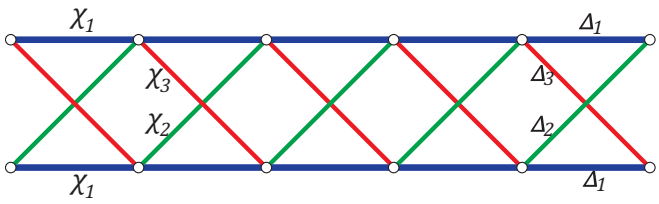

FIG. 7. The mean-field configuration in the model. Three kinds of bonds (blue, green, and red) and six different mean fields, $\chi_1, \chi_2, \chi_3, \Delta_1, \Delta_2, \Delta_3$, exist. In our solution the gap fields are $\Delta_1 = 0$, $\Delta_2 = -\Delta_3 > 0$, and the bond fields are $\chi_1 > 0$, $\chi_2 = \chi_3 = 0$.

difference of the mean fields between successive iterations is less than 10^{-3}. If we want to show the edge spins, we should generalize the formalism to an inhomogeneous system with OBCs and include local m_i.

B. Results

First, we consider the nonmagnetic case with periodic boundary conditions. $\Delta^{\nu}_{ij\sigma}$ and $\chi^{\nu}_{ij\sigma}$ are spin-independent mean fields. The self-consistent solution of the BdG equation gives us a superconducting state which is uniform in the x direction. The antiferromagnetic interaction J term exists in both intrachain nearest-neighbor sites (blue bonds in Fig. 7) and interchain next-nearest-neighbor sites (red and green bonds in Fig. 7). All these J terms can be decoupled into mean fields χ and Δ. In other words, we allow nonvanishing χ_1, χ_2, χ_3 and $\Delta_1, \Delta_2, \Delta_3$ in Fig. 7. However, in our self-consistent solution the gap fields $\Delta_1 = 0, \Delta_2 = -\Delta_3 > 0$. The bond fields $\chi_1 > 0$, $\chi_2 = \chi_3 = 0$. From the relative phase of the pair fields we confirm that the pairing symmetry is d_{xy}. To be specific, the gap fields satisfy $\Delta^{\nu}_{i,i+\hat{x}+\hat{y}} = -\Delta^{\nu}_{i,i-\hat{x}+\hat{y}} = \Delta^{\nu}$ if i sits on the lower chain and $\Delta^{\nu}_{i,i+\hat{x}-\hat{y}} = -\Delta^{\nu}_{i,i-\hat{x}-\hat{y}} = -\Delta^{\nu}$ if i sits on the upper chain. These results agree well with DMRG calculations. First, the pairing symmetries using the two distinct methods are identical. In addition, DMRG finds that $\langle c^{\dagger}_i c_j \rangle = 0$ when ij are two sites in the diagonal direction, and it is finite in the horizontal direction, which is the same as the χ field in the RMFT qualitatively.

The values of the two mean fields as a function of doping are depicted in Fig. 8(a). After multiplying g_t, the superconducting order parameter and bond order parameter are shown in Fig. 8(b). The pairing mean field Δ_2 decreases monotonically, and the order parameter Δ_{SC} forms a domelike shape. $\Delta_{SC} = g_t \Delta_2 = \frac{2\delta}{1+\delta}\Delta_2$ is roughly proportional to δ in the very low doping range, so that Δ_{SC} first increases with doping. After moderate doping the decrease in Δ_2 dominates over the increase in g_t. As a result, Δ_{SC} drops down along with the pairing field. The domelike behavior of the superconducting order parameter is similar to the results of the 2D and quasi-1D t-J model on a square lattice [11,23]. The bond order K increases monotonously as a function of doping because more doped holes may result in enhanced kinetic energies.

C. Momentum-space analyses

To give a further analysis of the problem, we switch to k space to obtain some relations between the mean fields. The mean-field Hamiltonian (10) can be written in momentum

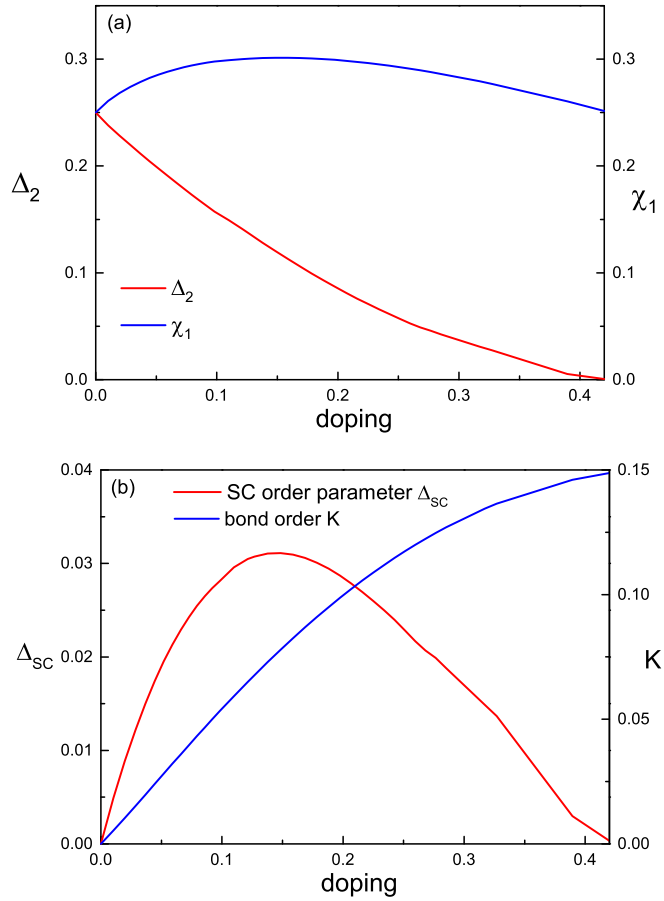

FIG. 8. (a) Pair field Δ_2 and bond field χ_1 as a function of doping concentration δ. (b) Superconducting order parameter Δ^{SC} and bond order K as a function of δ. SC order forms a domelike shape. (a) and (b) are the expectations of the operators in $|\Psi_0\rangle$ and $|\Psi\rangle$, respectively.

space as

$$H_k = \sum_{\boldsymbol{k},\sigma} \varepsilon_{\boldsymbol{k}} c^{\dagger}_{\boldsymbol{k},\sigma} c_{\boldsymbol{k},\sigma} + \sum_{\boldsymbol{k}} \widetilde{\Delta}_{\boldsymbol{k}} c^{\dagger}_{\boldsymbol{k}\uparrow} c^{\dagger}_{-\boldsymbol{k}\downarrow} + \text{H.c.}, \tag{11}$$

where

$$\varepsilon_{\boldsymbol{k}} = -2g_t t \cos k_x - \frac{3}{4} g_s J[2\chi_1 \cos k_x + \chi_2 \cos(k_x + k_y) + \chi_3 \cos(k_x - k_y)] - \mu, \tag{12}$$

$$\widetilde{\Delta}_{\boldsymbol{k}} = -\frac{3}{4} g_s J[2\Delta_1 \cos k_x + \Delta_2 \cos(k_x + k_y) + \Delta_3 \cos(k_x - k_y)]. \tag{13}$$

The mean fields $\chi_1, \chi_2, \chi_3, \Delta_1, \Delta_2, \Delta_3$ are shown in Fig. 7. First, we consider the half-filled case with $g_t = 0$. We can write $\varepsilon_{\boldsymbol{k}} = -3/4 g_s J \chi_{\boldsymbol{k}}$, $\widetilde{\Delta}_{\boldsymbol{k}} = -3/4 g_s J \Delta_{\boldsymbol{k}}$, with

$$\chi_{\boldsymbol{k}} = 2\chi_1 \cos k_x + \chi_2 \cos(k_x + k_y) + \chi_3 \cos(k_x - k_y) = 2\chi_1 \cos k_x + (\chi_3 + \chi_2) \cos k_x \cos k_y + (\chi_3 - \chi_2) \sin k_x \sin k_y, \tag{14}$$

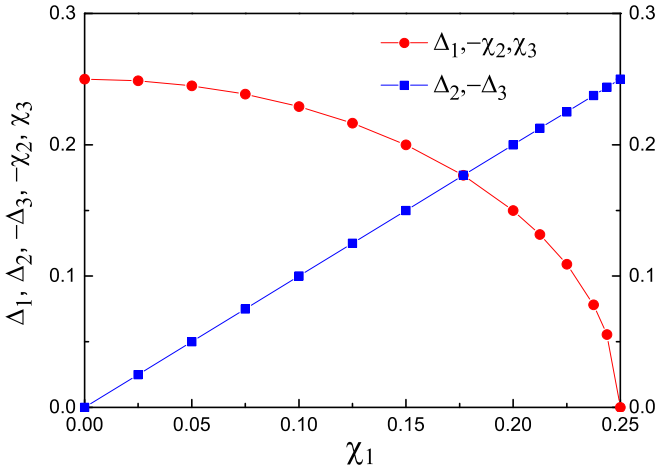

FIG. 9. The mean fields Δ_1, Δ_2, Δ_3, χ_2, χ_3 as a function of χ_1 in the half-filled case ($\delta = 0$). All of the points are the solutions of the BdG equation with exactly the same energy. They all satisfy the constraints (18), (19), and (20).

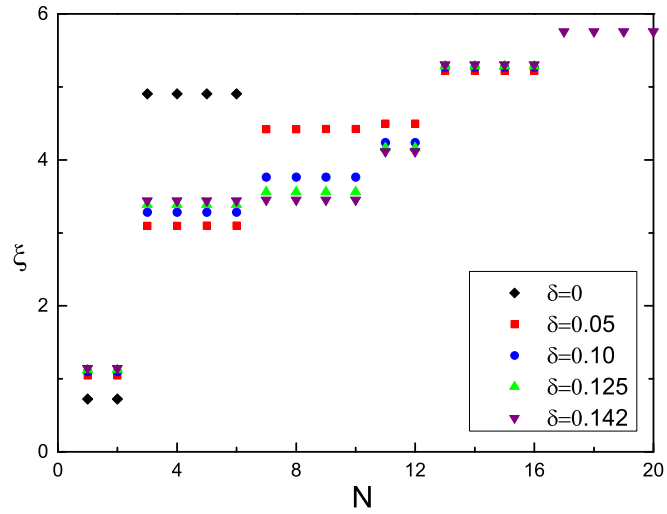

FIG. 10. The entanglement spectrum at different doping levels. Twofold degeneracy is the same as the undoped Haldane phase.

$$\begin{aligned}\Delta_{\boldsymbol{k}} &= 2\Delta_1 \cos k_x + \Delta_2 \cos(k_x + k_y) + \Delta_3 \cos(k_x - k_y)\\ &= 2\Delta_1 \cos k_x + (\Delta_3 + \Delta_2)\cos k_x \cos k_y\\ &\quad + (\Delta_3 - \Delta_2)\sin k_x \sin k_y. \end{aligned} \tag{15}$$

Using the same method with Refs. [11,23], we find that the energy of the system is

$$E = -\frac{3}{4} g_s J \sum_{\boldsymbol{k}} E_{\boldsymbol{k}}. \tag{16}$$

Here $E_{\boldsymbol{k}} = \sqrt{\chi_{\boldsymbol{k}}^2 + \Delta_{\boldsymbol{k}}^2}$. Inspired by the real-space solution, we can make an ansatz of $E_{\boldsymbol{k}}$,

$$E_{\boldsymbol{k}} = C\sqrt{4\cos^2 k_x + 4\sin^2 k_x \sin^2 k_y}, \tag{17}$$

where C is a parameter to be determined. Combining the expressions of $\chi_{\boldsymbol{k}}$ and $\Delta_{\boldsymbol{k}}$, we find that the mean fields should satisfy the following equations:

$$\chi_1^2 + \Delta_1^2 = \chi_2^2 + \Delta_2^2 = \chi_3^2 + \Delta_3^2 = C^2, \tag{18}$$

$$\chi_3 = -\chi_2, \Delta_3 = -\Delta_2, \tag{19}$$

$$\chi_1\chi_2 + \Delta_1\Delta_2 = 0. \tag{20}$$

Due to these constraints we have only one independent field. For example, if we fix χ_1, the absolute values of all mean fields are determined. Changing χ_1 will produce many states with the same energy. To verify these conditions, we calculate some ground states through solving the BdG equation (10) and show the mean fields in Fig. 9. With the increasing of χ_1, the fields $\Delta_1, -\chi_2, \chi_3$ decrease, and $\Delta_2, -\Delta_3$ increase. In addition, $\Delta_2 = -\Delta_3 = \chi_1$. These states indeed have same the energies, and they all satisfy the constraints (18), (19), and (20). The constant C equals 0.25. The degenerate states are all unprojected states. They correspond to the same projected RVB ground state [23].

When we slightly deviate from the half-filled case, the constraints above still hold approximately. Since the hopping term is only along the x direction, we should maximize χ_1 to make the absolute value of the kinetic energy as large as possible. As a result, $\chi_1 = C > 0$, $\Delta_1 = 0$ due to the constraint $\chi_1^2 + \Delta_1^2 = C^2$. In the diagonal direction, $\chi_2 = 0$ due to $\chi_1\chi_2 + \Delta_1\Delta_2 = 0$. Then $\Delta_2 = \pm C$ because $\chi_2^2 + \Delta_2^2 = C^2$. On the whole, the ground state is

$$\chi_1 = C, \quad \Delta_1 = 0, \quad \chi_2 = \chi_3 = 0, \quad \Delta_2 = -\Delta_3 = \pm C. \tag{21}$$

This is exactly the d_{xy}-wave superconducting state we calculated above using the DMRG and real-space RMFT method. $\chi_2 = \chi_3 = 0$ is also reasonable and same with the results before. However, $\chi_1 = \Delta_2 = C$ is satisfied only in the exactly half filled case, as shown by Fig. 8(a). Roughly speaking, d_{xy} superconductivity directly comes from J interaction in the diagonal bond, but it is the hopping term in the x direction that makes the system choose this ground state (the last point in Fig. 9). The success of the RMFT method in handling this problem demonstrates that the projected BCS function approach is efficient for describing d_{xy} superconductivity in the doped Haldane phase. The formalism of RVB can capture the essential physics in the present doped spin-1 system.

IV. DISCUSSION

A. Entanglement properties

The entanglement spectrum and entanglement entropy have been widely used to investigate various quantum systems [35]. The ground state of the spin-1 chain exhibits a twofold-degenerate entanglement spectrum [3], reflecting the nontrivial topological nature of the Haldane phase. We divide the diagonal ladder system with finite length L into two subblocks and calculate the eigenvalues w_α of the reduced density matrix $\rho_l = \mathrm{Tr}_{L-l}[\rho]$, with $l = L/2$. The entanglement spectrum $\xi_\alpha = -\ln w_\alpha$ at different dopings δ is shown in Fig. 10. When the system is in the half-filled state, the entanglement is almost the same as that for the spin-1 chain [3]. When we dope holes

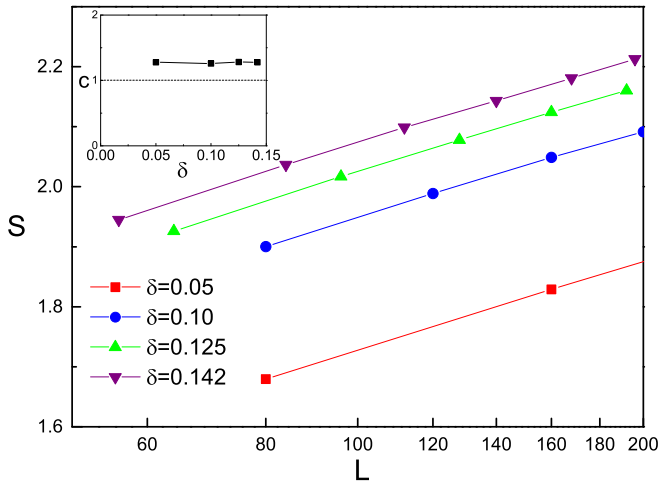

FIG. 11. The entanglement entropy S as a function of L at different doping levels. Inset: The central charge as a function of doping level.

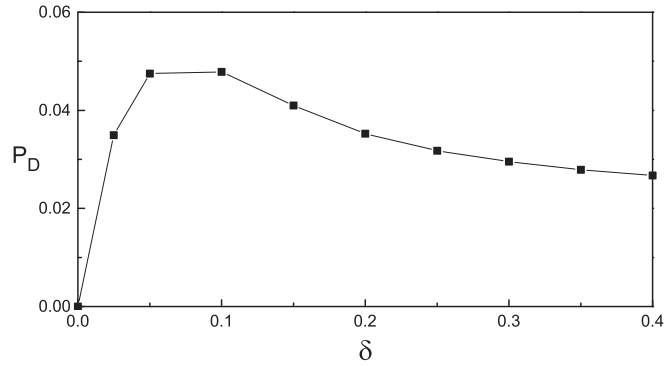

FIG. 12. The pairing correlation strength P_D as a function of doping δ in an 80×2 system. It first increases rapidly, then drops gradually.

into the system, twofold degeneracy still survives, which is consistent with the existence of edge states.

For $(1+1)$-dimensional critical systems the von Neumann entanglement entropy defined by $S = -\mathrm{Tr}\,\rho_l \ln \rho_l$ generally satisfies $S(L) = \frac{c}{6}\ln(L) + \tilde{c}$ [36]. Here c is the central charge in the conformal field theory, and $\tilde{c}$ is a constant in a specific model. The entanglement entropy as a function of L at different dopings δ is shown in Fig. 11. It is nearly a straight line. The inset shows the central charge c as a function of doping level δ determined from the fitting of S. In the Luther-Emery phase, the spin sector is gapped, and there is a single gapless mode in the charge sector. The central charge is expected to be 1. Our calculations show that the central charge is close to but slightly larger than $c = 1$, similar to some previous calculations using the same method [31]. These results demonstrate that our ground state is a Luther-Emery liquid.

B. Comparison of DMRG and RMFT results

We have shown that qualitatively the same results can be obtained by using the RMFT and DMRG methods in this quasi-1D system. However, the RMFT method generates finite pairing order, and the DMRG method has power-law decaying quasi-long-range order. To reveal the pairing strength in the DMRG, we averaged the correlation function in the interior region of the system for a fixed r to minimize the influences of edge states:

$$P(r) = \frac{1}{L/2 - r - 1} \sum_{j=L/4+1}^{3L/4-r-1} \left\langle \hat{\Delta}^{s}_{x+y}(j)\hat{\Delta}^{s}_{x+y}(j+r)^{\dagger} \right\rangle. \quad (22)$$

Then we summed over many different r to estimate the pairing correlation strength in this system [37]. In Fig. 12 we show $P_D = \sum_{r=4}^{38} P(r)$ as a function of doping in an 80×2 system using $m = 1000$ DMRG states. We find that P_D increases rapidly with hole doping starting from the half-filled case and reaches a maximum at around $\delta = 0.1$. Then it decreases gradually in a wide doping range. The concrete values depend on the lower and upper bounds in the sum, but the overall tendency is insensitive to them. The doping evolution is qualitatively similar to the dome shape calculated using the RMFT in Fig. 8(b) and consistent with the behavior of the binding energy shown in Fig. 3. It seems that the pairing strength does not drop to zero when $\delta = 0.4$. The possible finite pairing correlations when $\delta > 0.4$ are beyond the consideration of this paper.

To make further comparisons with these two methods, we calculate the ground-state energy and the superexchange energy per site. Here we introduce a new Gutzwiller factor to improve the approximation by

$$g_s = \frac{4n^2}{n^2(1+\delta)^2 + 8\delta^2(|\Delta|^2 - |\chi|^2) + 16(|\Delta|^4 + |\chi|^4)},$$

where $n = 1 - \delta$. This modification has been used to study the two-leg square t-J model [11]. The mean fields and the order parameter are almost unchanged compared to the common Gutzwiller factor, but the superexchange energy is closer to the result of the DMRG at most doping levels (shown in Fig. 13). The total energy shown in the inset of Fig. 13 still slightly deviates from the DMRG result when holes are doped into the system. The modifications of g_t in Ref. [11] are not useful to obtain more accurate energy. In the DMRG calculation, we consider the middle part of the system ($L/4$ to $3L/4$) to reduce boundary effects. Generally speaking, the RMFT can obtain energies quite close to those of the DMRG method.

In addition to the superconducting properties, the RMFT results can also reveal the edge state under the condition of the OBCs. The expectation value of S^z_i is represented by m_i. By taking into account m_i, the RMFT calculations become a little more complicated with modifications of renormalized Gutzwiller factors [38,39]. Here we add an external Zeeman field $-h(n_i\uparrow - n_i^{\downarrow})$ to drive the system to the $S = 1$ sector. The expectation of S^z_i at different sites is shown in Fig. 14. The length of the system is 100, and the doping level is 0.15. For comparison, the DMRG results are shown in the inset. These two methods present quite similar features in which the edge spins $S_b = 1/2$ and S^z_i decays to zero in the bulk of the system. It shows that the RMFT method can describe the main physics of the present model.

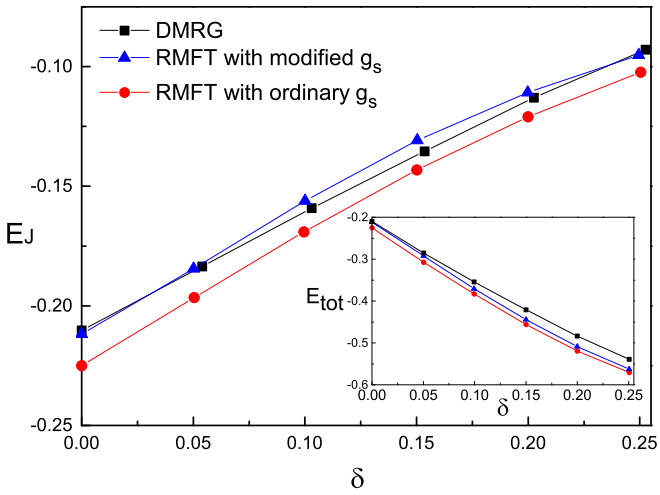

FIG. 13. The superexchange energy per site at several doping levels using different methods in a 100×2 system. Inset: The total energy per site using different methods. The energies of RMFT with modified g^s are closer to those of DMRG.

C. Effects of J/t

In this section we briefly discuss the effects of J/t in the $0.1 \leqslant J/t \leqslant 0.5$ regime ($t = 1.0$ is fixed). According to our analyses before, pairing strength would increase with J because it directly comes from the mean-field decoupling of the antiferromagnetic interaction. In Fig. 15 we show the pairing strength as a function of J/t in an 80×2 system using the DMRG and RMFT methods. In the DMRG method, we calculate the pair-pair correlation function P_D. In the RMFT method we calculate the superconducting order parameter Δ_{SC} defined in (9). Both methods exhibit a continuous increasing of the pairing strength with J, as expected, showing the consistency of the two methods.

Besides pairing strength, we also calculate the spin gap and binding energy as a function of J/t in Fig. 16 with

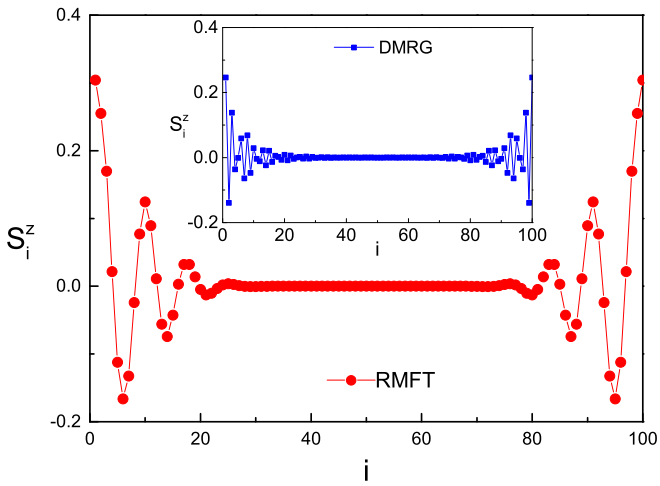

FIG. 14. The spatial distribution of S^z using the RMFT method in a 100×2 system with doping $\delta = 0.15$ in the sector $S^z_{tot} = 1$. Inset: S^z_i using the DMRG method in the same system. Edge state $S = 1/2$ appears in both methods.

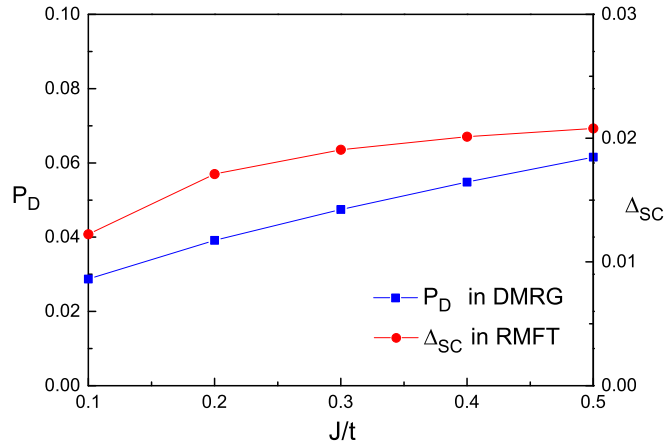

FIG. 15. The pairing strength as a function of J/t calculated using DMRG and RMFT. Both methods show that larger J makes the pairing stronger, as expected.

$L = 80$ using the DMRG method. The spin gap divided by J is shown on the left axis. $\Delta_{S=1}$ is always zero due to the gapless edge states. $\Delta_{S=2}/J$ only slightly changes with J/t because the antiferromagnetic Heisenberg terms control the bulk Haldane gap. The binding energy E_b shown on the right axis is negative, and its absolute value increases with J/t, which is consistent with the increasing pairing strength. These results show that the value of J/t does not change the properties of the doped Haldane phase qualitatively, at least in the $0.1t \leqslant J \leqslant 0.5t$ regime.

D. d_{xy}-wave superconductivity in other models

We note that d_{xy}-wave superconductivity has been found in several Hubbard or (t-J)-type ladder models [15–19]. In our opinion their low-energy physics is almost the same as in this paper. To achieve this kind of superconductivity, first, we need an intrachain hopping term. Then we need an effective antiferromagnetic Heisenberg interaction between horizontal

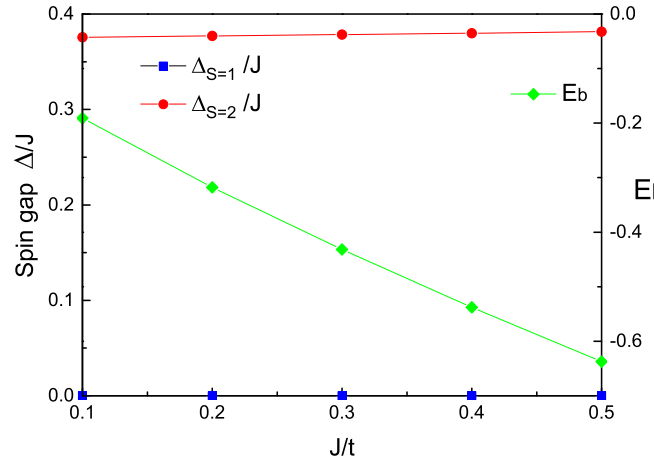

FIG. 16. The spin gap $\Delta_{S=1}/J$, $\Delta_{S=2}/J$ (left axis) and binding energy E_b (right axis) as a function of J/t in an 80×2 system. The spin gap only slightly changes with J/t. The binding energy E_b becomes more negative with the increasing of J/t.

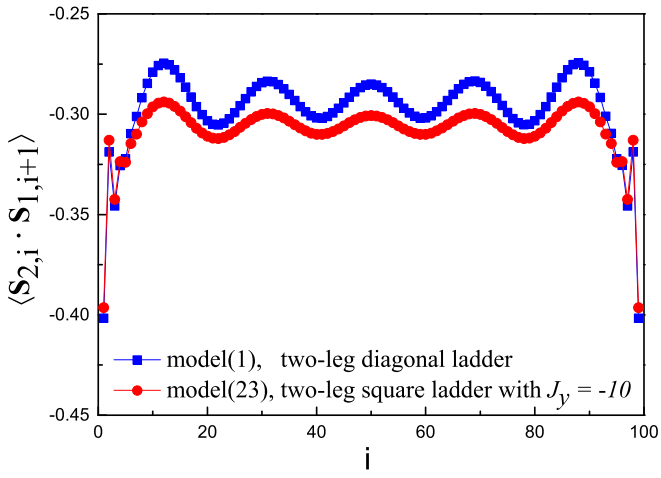

FIG. 17. The spin-spin correlation function in the diagonal direction in models (1) and (23). The system is a 100×2 ladder with doping level $\delta = 0.05$. We can see that both models have a strong antiferromagnetic correlation. The model (23) has no direct J interaction in the direction, but the correlation is even stronger than model (1).

neighboring sites. This interaction can also be induced by the on-site Hubbard U term and intrachain hopping t. Finally, we need a coupling between two chains. A vertical ferromagnetic term or a diagonal antiferromagnetic term will work. For example, d_{xy}-wave superconductivity appears in the doped two-leg ladder model in Refs. [15,16]. The Hamiltonian is

$$H = -t \sum_{i\sigma} (c^{\dagger}_{1,i,\sigma} c_{1,i+1,\sigma} + c^{\dagger}_{2,i,\sigma} c_{2,i+1,\sigma}) + \text{H.c.} + J_x \sum_i (\boldsymbol{S}_{1,i} \cdot \boldsymbol{S}_{1,i+1} + \boldsymbol{S}_{2,i} \cdot \boldsymbol{S}_{2,i+1}) + J_y \sum_i \boldsymbol{S}_{1,i} \cdot \boldsymbol{S}_{2,i}. \tag{23}$$

Here $t = 1, J_x = 0.3, J_y = -10$. The J_x term is the intrachain antiferromagnetic Heisenberg interaction. The J_y term couples two sites at different chains with a strong ferromagnetic interaction. The ground state has a remarkable spin-spin correlation in the diagonal direction, shown as red points in Fig. 17, very similar to the correlation function shown as blue points in the model (1) with the direct J term in that direction. The oscillation is induced by the charge density Friedel oscillations discussed before. We conclude that the low-energy effective Hamiltonian of the present model may contain an effective antiferromagnetic Heisenberg interaction along the diagonal direction, which leads to the d_{xy}-wave pairing.

E. Changing the hopping term

In this section, we provide more pieces of evidence to support our arguments that the ground state is determined by how the electrons hop in the ladder system. In model (1) the hopping term is along the intrachain bond. Now we change the hopping term to

$$H = t \sum_{i,\sigma} (c^{\dagger}_{1,i,\sigma} c_{2,i+1,\sigma} - c^{\dagger}_{2,i,\sigma} c_{1,i+1,\sigma} + \text{H.c.}). \tag{24}$$

It means that the hopping term is along the diagonal direction and the hopping matrix elements are t and $-t$ in the two directions. Like in the analysis above, to maximize the absolute value of the kinetic energy we should force $\chi_2 = -\chi_3 = C > 0$. As a result, $\Delta_2 = \Delta_3 = 0$, $\chi_1 = 0$, $\Delta_1 = \pm C$. This state is just the first point in Fig. 9 with uniform pairing in the intrachain bonds at both chains. The real-space RMFT and DMRG results show that pairing order or quasi-long-range correlation indeed appears in the intrachain bond in the ground state. d_{xy} pairing symmetry no longer exists. Meanwhile, the finite expectation value of $c^{\dagger}_i c_j$ appears in the diagonal direction instead of the horizontal direction. In addition, both methods show that the ground-state energies of this model and model (1) are the same. These results further demonstrate our earlier statements. Pairing order Δ and bond order χ can appear in all bonds with J interaction. It is the hopping term that determines their behavior and the real ground state.

V. SUMMARY

We proposed a doped two-leg diagonal ladder model to realize the doped Haldane phase with a dominant d_{xy}-wave pairing correlation. By using the DMRG method, we found that the ground state hosts some common features of the Haldane phase, including the spin gap, edge states, and twofold degeneracy in the entanglement spectrum. From the Friedel oscillation and the power-law decaying pair-pair correlation, we confirmed that the ground state belongs to Luther-Emery liquid with the Luttinger parameter $K_\rho > 1$. In addition, we used the Gutzwiller approximation and decoupled the J term to get bond and pair mean fields in the framework of the RMFT. The superconducting order parameter with d_{xy}-wave symmetry was obtained, which originates from the antiferromagnetic interaction in the diagonal direction. The intrachain hopping term may stabilize this state. The superconducting order parameter forms a domelike shape as a function of the doping levels. Even though the RMFT method is at the mean-field level, its results, including the superconducting pairing symmetry, the evolution of pairing strength as a function of doping, ground-state energy, and the presence of edge states, agree well with those of the numerically exact DMRG method. These results clearly show that the RMFT method based on the RVB picture works quite well in the present diagonal ladder model. When we change the value of J/t, the ground state is qualitatively invariant, and the pairing strength increases with J.

Fe-based superconductivity has attracted much attention during the past decade. Our results may be relevant in two aspects. First, the superconductivity in ladder compound $BaFe_2S_3$ is explained regarding a two-orbital Hubbard model [19]. Our model shows the same pairing symmetry as their model and can be treated as an effective model in the large-U limit. Second, it is widely believed that the magnetism of FeSe should be explained with models with spin-1 local moments [40,41]. Then it is promising to generalize our effective spin-1 chain to a two-dimensional spin-1 model to explore the superconductivity in the FeSe system.

ACKNOWLEDGMENTS

We thank Z. Y. Weng for helpful discussions. This work was supported by the National Key Research and Development Program of China (Grants No. 2017YFA0304204 and No. 2016YFA0300504) and the National Natural Science Foundation of China (Grants No. 11625416 and No. 11474064).

[1] F. D. M. Haldane, Phys. Lett. A **93**, 464 (1983).
[2] S. R. White and D. A. Huse, Phys. Rev. B **48**, 3844 (1993).
[3] F. Pollmann, A. M. Turner, E. Berg, and M. Oshikawa, Phys. Rev. B **81**, 064439 (2010).
[4] Q.-R. Wang and P. Ye, Phys. Rev. B **90**, 045106 (2014).
[5] A. Keselman, E. Berg, and P. Azaria, Phys. Rev. B **98**, 214501 (2018).
[6] T. M. Rice, Z. Phys. B **103**, 165 (1997).
[7] Y.-F. Jiang, H.-C. Jiang, H. Yao, and S. A. Kivelson, Phys. Rev. B **95**, 245105 (2017).
[8] S. R. White, Phys. Rev. Lett. **69**, 2863 (1992).
[9] U. Schollwöck, Rev. Mod. Phys. **77**, 259 (2005).
[10] E. Dagotto, J. Riera, and D. Scalapino, Phys. Rev. B **45**, 5744 (1992).
[11] M. Sigrist, T. M. Rice, and F.-C. Zhang, Phys. Rev. B **49**, 12058 (1994).
[12] D. Poilblanc, D. J. Scalapino, and S. Capponi, Phys. Rev. Lett. **91**, 137203 (2003).
[13] S. R. White, D. J. Scalapino, and S. A. Kivelson, Phys. Rev. Lett. **115**, 056401 (2015).
[14] K. Hida, J. Phys. Soc. Jpn. **64**, 4896 (1995).
[15] H.-C. Jiang, Z.-X. Li, A. Seidel, and D.-H. Lee, Sci. Bull. **63**, 753 (2018).
[16] Z. Zhu, D. N. Sheng, and Z. Y. Weng, Phys. Rev. B **97**, 115144 (2018).
[17] B. Ammon and M. Imada, J. Phys. Soc. Jpn. **69**, 1946 (2000).
[18] T. Shirakawa, S. Nishimoto, and Y. Ohta, Phys. Rev. B **77**, 224510 (2008).
[19] N. D. Patel, A. Nocera, G. Alvarez, A. Moreo, and E. Dagotto, Phys. Rev. B **96**, 024520 (2017).
[20] S. R. White, Phys. Rev. B **53**, 52 (1996).
[21] G. Fath, O. Ligeza, and J. Solyom, Phys. Rev. B **63**, 134403 (2001).
[22] A. Luther and V. Emery, Phys. Rev. Lett. **33**, 589 (1974).
[23] F. C. Zhang, C. Gros, T. M. Rice, and H. Shiba, Supercond. Sci. Technol. **1**, 36 (1988).
[24] P. W. Anderson, Science **235**, 1196 (1987).
[25] J. Y. Gan, Y. Chen, Z. B. Su, and F. C. Zhang, Phys. Rev. Lett. **94**, 067005 (2005).
[26] B. Edegger, V. N. Muthukumar, and C. Gros, Adv. Phys. **56**, 927 (2007).
[27] M. Raczkowski and D. Poilblanc, Phys. Rev. Lett. **103**, 027001 (2009).
[28] S. Wang, L. Zhang, and F. Wang, Phys. Rev. B **97**, 035112 (2018).
[29] ITENSOR, http://itensor.org/.
[30] M. A. Cazalilla, J. Phys. B **37**, S1 (2004).
[31] H.-C. Jiang, Z.-Y. Weng, and S. A. Kivelson, Phys. Rev. B **98**, 140505 (2018).
[32] M. Dolfi, B. Bauer, S. Keller, and M. Troyer, Phys. Rev. B **92**, 195139 (2015).
[33] K. Kobayashi, M. Okumura, S. Yamada, M. Machida, and H. Aoki, Phys. Rev. B **94**, 214501 (2016).
[34] M. Troyer, H. Tsunetsugu, and T. M. Rice, Phys. Rev. B **53**, 251 (1996).
[35] N. Laflorencie, Phys. Rep. **646**, 1 (2016).
[36] P. Calabrese and J. Cardy, J. Phys. A **42**, 504005 (2009).
[37] R. M. Noack, N. Bulut, D. J. Scalapino, and M. G. Zacher, Phys. Rev. B **56**, 7162 (1997).
[38] K.-Y. Yang, W.-Q. Chen, T. M. Rice, M. Sigrist, and F.-C. Zhang, New. J. Phys. **11**, 055053 (2009).
[39] W.-L. Tu and T. K. Lee, Sci. Rep. **6**, 18675 (2016).
[40] F. Wang, S. A. Kivelson, and D.-H. Lee, Nat. Phys. **11**, 959 (2015).
[41] S.-S. Gong, W. Zhu, D. N. Sheng, and K. Yang, Phys. Rev. B **95**, 205132 (2017).